

Antarctic Surface and Subsurface Snow and Ice Melt Fluxes

GLEN E. LISTON

Department of Atmospheric Science, Colorado State University, Fort Collins, Colorado

JAN-GUNNAR WINTHER

Norwegian Polar Institute, Polar Environmental Centre, Tromsø, Norway

(Manuscript received 19 April 2004, in final form 22 October 2004)

ABSTRACT

This paper presents modeled surface and subsurface melt fluxes across near-coastal Antarctica. Simulations were performed using a physical-based energy balance model developed in conjunction with detailed field measurements in a mixed snow and blue-ice area of Dronning Maud Land, Antarctica. The model was combined with a satellite-derived map of Antarctic snow and blue-ice areas, 10 yr (1991–2000) of Antarctic meteorological station data, and a high-resolution meteorological distribution model, to provide daily simulated melt values on a 1-km grid covering Antarctica. Model simulations showed that 11.8% and 21.6% of the Antarctic continent experienced surface and subsurface melt, respectively. In addition, the simulations produced 10-yr averaged subsurface meltwater production fluxes of 316.5 and 57.4 km³ yr⁻¹ for snow-covered and blue-ice areas, respectively. The corresponding figures for surface melt were 46.0 and 2.0 km³ yr⁻¹, respectively, thus demonstrating the dominant role of subsurface over surface meltwater production. In total, computed surface and subsurface meltwater production values equal 31 mm yr⁻¹ if evenly distributed over all of Antarctica. While, at any given location, meltwater production rates were highest in blue-ice areas, total annual Antarctic meltwater production was highest for snow-covered areas due to its larger spatial extent. The simulations also showed higher interannual meltwater variations for surface melt than subsurface melt. Since most of the produced meltwater refreezes near where it was produced, the simulated melt has little effect on the Antarctic mass balance. However, the melt contribution is important for the surface energy balance and in modifying surface and near-surface snow and ice properties such as density and grain size.

1. Introduction

It is generally accepted that the Antarctic ice sheet consists largely of accumulation zones that experience no melting during the annual cycle. However, melt-related features have been observed in some areas near the margin. This melting has been typically found in areas with favorable climate conditions (e.g., relatively high air temperatures and strong incoming solar radiation), such as on the sub-Antarctic islands (e.g., Birnie and Gordon 1980), on the ice shelves and snow areas of the Antarctic Peninsula (e.g., Ridley 1993; Scambos et al. 2000; Fahnestock et al. 2002; Rau and Braun 2002; Shepherd et al. 2003), and in the McMurdo “Dry Valleys” (e.g., Chinn 1993; Fountain et al. 1998; Lewis et al. 1998; Dana et al. 2002). Melt features have also been observed and simulated on the ice shelves and near the

coast of East Antarctica (Phillips 1998; van den Broeke et al. 2005), on the McMurdo Ice Shelf (Paige 1968), and on the Ross Ice Shelf (Jezek 1999). In addition to favorable atmospheric conditions, the snow and ice itself can influence melt production. In many areas of Antarctica, blue-ice areas exist that are characterized by a negative mass balance (Bintanja 1999). These areas typically have relatively large ice grains and low albedo that can enhance local melt production (e.g., Bøggild et al. 1995; Winther et al. 1996; Liston et al. 1999b). In Dronning Maud Land, East Antarctica, such areas are often found close to nunataks (Orheim and Lucchitta 1990). To help understand the significance of these melt features, satellite microwave data have been used to monitor and quantify Antarctic melt season duration and spatial extent (Zwally and Fiegles 1994; Bingham and Drinkwater 2000; Torinesi et al. 2003).

In addition to the traditional concept of snow and ice melting at the surface in response to favorable air temperatures and the snow–ice surface energy budget, a second mechanism can produce Antarctic meltwater

Corresponding author address: Dr. Glen E. Liston, Dept. of Atmospheric Science, Colorado State University, Fort Collins, CO 80523-1371.
E-mail: liston@atmos.colostate.edu

fluxes. Colbeck (1989) and Brandt and Warren (1993) implemented theoretical snow temperature studies describing the possibility of a temperature maximum below the surface, that is, the “solid-state greenhouse” caused by solar radiation penetration and absorption within the snow–ice and the restriction of longwave radiative cooling at the snow–ice surface. Brandt and Warren (1993) concluded that, while the solid-state greenhouse within snow was uncertain, subsurface blue-ice melting would likely occur due to the smaller extinction coefficients and lower albedo of ice. In the high-elevation mountains of Bolivia, Hardy et al. (2001) observed a thin ice layer 20 cm below the snow surface that they attributed to subsurface melting and refreezing. Brun et al. (1989) observed and simulated temperature maxima below an alpine snow surface. In another study of this solid-state greenhouse in seasonal snow, Koh and Jordan (1995) combined high-resolution radar observations with a one-dimensional mass and energy balance model and concluded that subsurface melt in low-density snow is likely under conditions of calm, clear days when air temperatures are near but below freezing.

For the last ten years, using a combination of field investigations, satellite studies, and model developments and simulations, we have studied subsurface melt of the type described by Brandt and Warren (1993) in the Jutulgryta snow and blue-ice fields located in coastal Dronning Maud Land. This area is located on the land-ice mass 70 km away from the nearest nunatak and 130 km from the ice shelf barrier at elevations between 150 and 300 m MSL. In Jutulgryta, subsurface melt features are found in both snow and blue-ice areas; they appear below a relatively undisturbed frozen surface (the surface is commonly cold and dry with no evidence of any surface melting). This lack of melt-related surface features makes the subsurface melt difficult to detect from space (Winther 1993), and also makes it difficult to detect while actually standing on the snow and blue-ice surfaces (although if you are very quiet you can often hear meltwater percolating through the blue ice). The subsurface snow area melt is generally subtle, while the subsurface blue-ice area melt can be dramatic (Fig. 1). The hidden nature of the subsurface melt features generally requires digging below the surface to detect the associated liquid water, ice lenses, water flow, and other melt-related features (Bøggild et al. 1995; Winther et al. 1996; Liston et al. 1999b). The widespread spatial extent of these subsurface melt areas was first discovered during the 1993/94 Norwegian Antarctic Research Expedition (NARE) when a snow machine broke through the surface ice and was stuck in a 0.5-m-deep layer of water and ice.

After discovery of the Jutulgryta subsurface melt phenomenon, we intensified our field measurements and energy-balance modeling studies. A physically based numerical model of the coupled atmosphere, radiation, snow and blue-ice system was developed and

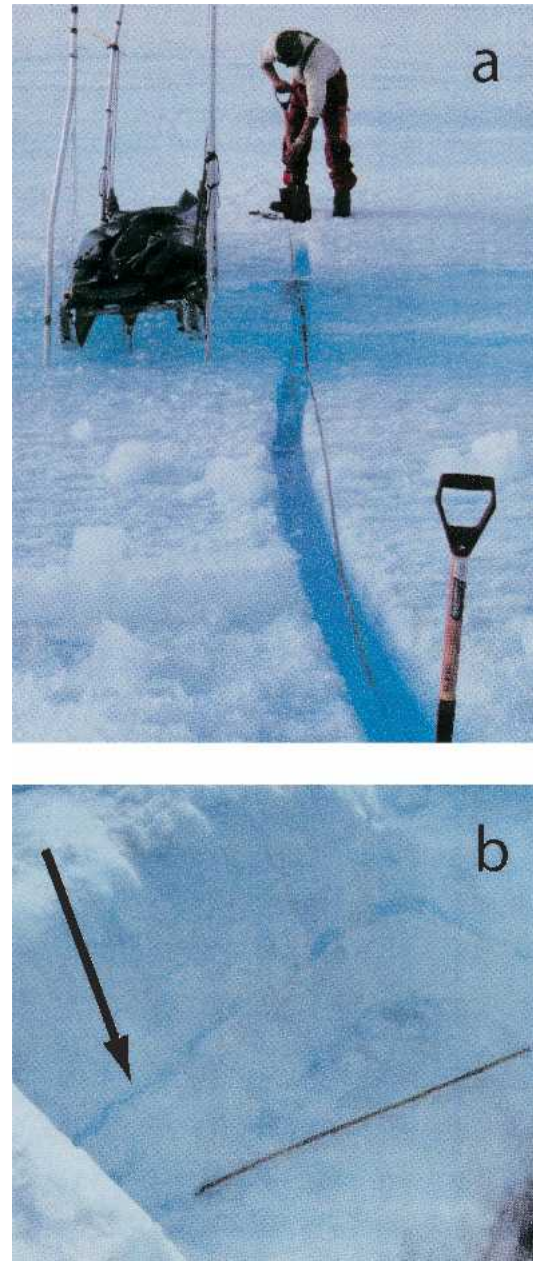


FIG. 1. Photographs from Jutulgryta, Dronning Maud Land, East Antarctica, showing evidence of subsurface melt. (a) A 10-m-long groove cut in the blue-ice surface with a chainsaw, exposing a 0.25-m deep meltwater channel below 10 cm of ice. (b) A 60-cm-deep pit in snow, showing a 5-cm-thick ice lens located 40 cm below the surface (identified by the black arrow); we observed these lenses to be continuous throughout the length of 15-m-long snow trenches and found no evidence of water percolation columns that would indicate meltwater transport from the surface of the snowpack. Liston et al. (1999b) concluded that the only way these could form was by penetration of solar radiation. The ruler in the bottom of the snow pit is 60 cm long.

tested against our field observations (Liston et al. 1999b). Model simulations suggested that the observed differences between subsurface snow and blue-ice melting could be largely explained by the radiative and heat

transfer interactions resulting from differences in albedo, grain size, and density between the two mediums. Because of the delicate balances between ice temperature, solar radiation, and the melting temperature the melt-related fluxes are sensitive to atmospheric conditions of air temperature and cloud-cover fraction (Liston et al. 1999a). In addition, katabatic winds limit winter snow accumulation and further support the presence of blue ice (Liston et al. 2000). In Jutulgryta, if we assume that the subsurface blue-ice meltwater does not drain away from the local area, the summer meltwater typically refreezes in early May. To our knowledge, Jutulgryta represents the first place on the Antarctic continent where extensive subsurface melt in both snow and blue-ice has been observed, analyzed, and reproduced with a numerical model.

Because of the clear role that blue ice plays in the existence of Antarctic melt processes, our long-term goal of calculating continental-scale meltwater fluxes required us to identify and map all Antarctic blue-ice locations. Winther et al. (2001) accomplished this by analyzing the National Oceanic and Atmospheric Administration (NOAA) Advanced Very High Resolution Radiometer (AVHRR) nearly cloud-free mosaic covering the Antarctic continent. Using this mosaic we were able to discriminate between three types of blue ice: “melt induced,” “wind induced,” and “potential.” The spatial distributions of these ice features were mapped over the $1.01 \text{ km} \times 1.01 \text{ km}$ mosaic grid and yielded a conservative Antarctic blue-ice area coverage estimate of $120\,472 \text{ km}^2$ (approximately 0.9% of the Antarctic continent), with a potential maximum of $239\,902 \text{ km}^2$ (approximately 1.7% of the Antarctic continent).

In what follows, we combine the satellite-derived blue-ice areas reported by Winther et al. (2001) and the energy balance model developed by Liston et al. (1999b), with 10 years of Antarctic climatological data (Fig. 2), to estimate surface and subsurface meltwater fluxes throughout Antarctica. In contrast to most current assumptions, we show that Antarctica surface and subsurface melt is important in both extent and magnitude.

2. Methods

As part of the 1996/97 NARE to Dronning Maud Land, a physically based numerical model of the coupled atmosphere, radiation, snow, and blue-ice system was developed that simulates the surface and subsurface (or near surface) melt in Antarctic blue-ice and snow areas (Liston et al. 1999b). The model comprises a heat transfer equation that includes a spectrally dependent solar radiation source term. The penetration of radiation into the snow and blue ice depends on the solar radiation spectrum, the surface albedo, and the snow and blue-ice grain sizes and densities. In addition,

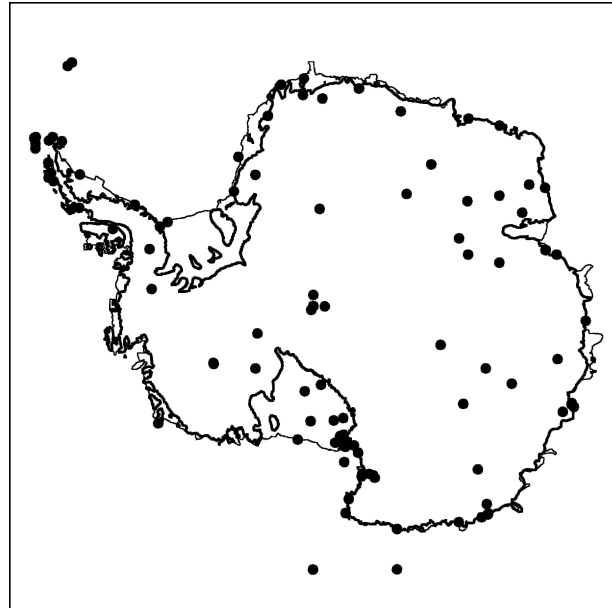


FIG. 2. Locations of the 106 GSOD Antarctic meteorological stations used in the model simulations (solid dots). The thick line defines the continental outline, and the fine lines define the ice shelves.

the model uses a complete surface energy balance to define the upper snow and blue-ice surface boundary conditions. The model can be run over the full annual cycle, simulating temperature profiles and melting and freezing quantities throughout the summer and winter seasons (Fig. 3). The modeling system, and its validation, make use of field observations collected during the 1996/97 NARE (Liston et al. 1999b).

a. Model description

The Liston et al. (1999b) model simulates the one-dimensional, time-dependent temperature and melting distributions within an ice sheet having characteristics that allow penetration of solar radiation into its upper layers. The formulation relies heavily on the methods of Schlatter (1972) who developed a model to study the subsurface temperature and melt profiles in Antarctica using a broadband (spectrally independent and constant with depth) solar radiation extinction coefficient. In addition, the formulation makes strong use of the techniques developed by Brandt and Warren (1993), who modified Schlatter's methodology to include the spectral dependence of solar radiation penetrating snow and ice. Brandt and Warren (1993) concluded that this spectral dependence is required to correctly describe the subsurface energy exchanges. In addition, they suggested that significant radiative heating differences are possible under conditions of dense snow and blue ice.

Energy is transferred through the snow–ice–water

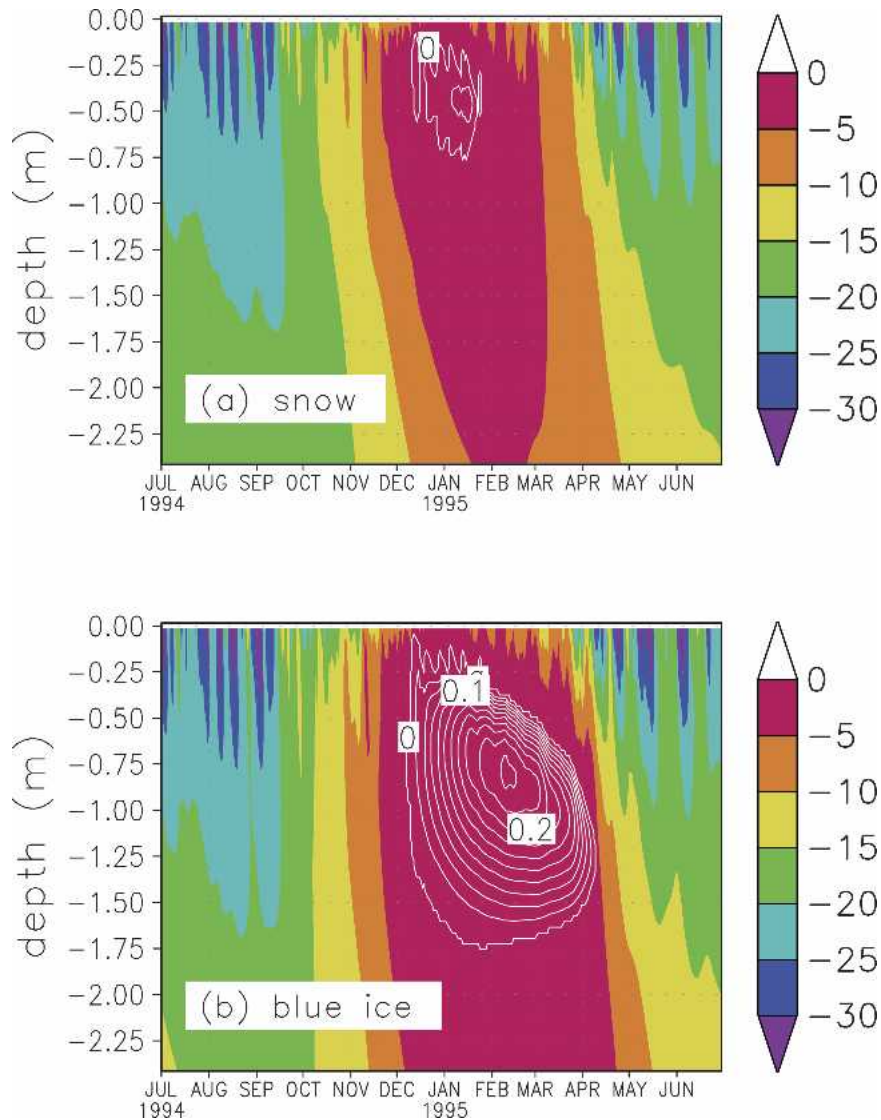


FIG. 3. Simulated Jutulgyta annual temperature evolution (color bands, °C) in the top 2.5 m for (a) snow and (b) blue ice. Also included is the water fraction, plotted using white contours ranging from 0.0 to 0.225 in intervals of 0.025. Adapted from Liston et al. (1999b).

matrix by conduction along grain boundaries and by vapor diffusion along pore spaces. In addition, this problem requires a solar radiation energy source term that varies with depth. The general ice temperature distribution and temporal evolution are described by the following one-dimensional heat transfer equation:

$$\rho_i C_p \frac{\partial T_i}{\partial t} = \frac{\partial}{\partial z} \left((k_i + k_v) \frac{\partial T_i}{\partial z} \right) - \frac{\partial q}{\partial z}, \quad (1)$$

where T_i is the snow/ice temperature, z is the vertical coordinate, t is time, ρ_i is the snow/ice density, C_p is the specific heat of the snow/ice, k_i is the thermal conductivity of the snow/ice matrix, k_v is a latent heat flux coefficient, and q is the solar-radiative flux. The radia-

tion flux penetrating the snow or ice, q , is computed using a two-stream approximation following Schlatter (1972). In this formulation, when the downward solar flux passes through a layer, dz , it is reduced by absorption and upward reflection, and enhanced by downward reflection of the upward flux.

The solution of Eq. (1) requires top and bottom boundary conditions and initial conditions. The top boundary condition is determined by performing a full energy balance at the surface in the form:

$$(1 - \alpha) Q_{si} + Q_{li} + Q_{le} + Q_h + Q_e + Q_c = Q_m, \quad (2)$$

where α is the surface albedo, Q_{si} is the solar (short-wave) radiation reaching the surface of the earth, Q_{li} is

the incoming longwave radiation, Q_{le} is the emitted longwave radiation, Q_h is the turbulent exchange of sensible heat, Q_e is the turbulent exchange of latent heat, Q_c is the conductive energy transport, and Q_m is the energy flux available for melt. Details of this surface energy balance formulation are provided in Liston et al. (1999b), where each term in Eq. (2) is cast in a form that leaves the surface temperature, T_o , as the only unknown. Equation (2) is then solved for T_o , which is used as the top boundary condition for Eq. (1).

By making the model domain sufficiently deep so that the temperature profile is independent of depth and time in the lowest few meters of the domain over a full annual cycle, the bottom boundary condition is

$$\left. \frac{dT_i}{dz} \right|_{z_{\max}} = 0, \quad (3)$$

where annual model integrations show this condition to be valid at $z_{\max} = 15$ m. For the simulations considered in this paper, initial conditions throughout the profile, for each grid cell, are given by imposing a constant snow/ice temperature profile equal to the 10-yr, mean annual air temperature and then integrating the model starting on 1 July. Equation (1), in conjunction with the boundary conditions defined by Eqs. (2) and (3), are solved using a finite control-volume methodology with a 3-cm grid increment over the 15-m vertical domain (Liston et al. 1999b).

As part of the model solution, the melting of ice and refreezing of water are handled by a water-fraction computation. Each model grid cell is assumed to have a water fraction and an ice fraction that sum to unity. Snow/ice temperatures computed above 0°C are reset to 0°C and the temperature difference is used to determine the melt energy and resulting meltwater produced, expressed as a fraction of the grid cell. The temperature profile is then recomputed while forcing the 0°C temperatures to remain fixed. During the freeze-up of grid cells containing a nonzero water fraction, computed temperatures below 0°C are used to determine the “cold energy” available to freeze the remaining liquid. Additional cold energy available after the liquid fraction has been reduced to zero goes toward reducing the temperature below 0°C . This methodology conserves energy, while maintaining the condition that liquid water existing in the presence of ice cannot rise above 0°C . Because the snow/ice at some point below

any simulated melt layer is typically below 0°C , the model assumes that any meltwater is refrozen in the same area where it was formed (e.g., there is no lateral transport to the ocean).

b. Model inputs

To solve the model system of equations, additional information is required in the form of atmospheric forcing data, snow and blue-ice distribution data, snow and blue-ice property data, and the distributions of parameters describing the interaction between snow and ice grains and solar radiation. The solar-related parameter distributions used in the simulations are described in Liston et al. (1999b). Snow and ice property data are required in the form of spectrally integrated albedo, density, and grain size. To define parameter values for the simulations presented herein, we separated our simulation domain into two distinct regions: elevations below 150 m and elevations above 1500 m. We assumed that it was appropriate for elevations of 150 m and below to have “coastal” snow parameter values and elevations of 1500 m and above to have “interior” snow values. Coastal snow values were defined to be equal to those used by Liston et al. (1999b) for Jutulgryta (elevation 150 m). Interior snow albedo values were defined following Grenfell et al. (1994), Winther (1994), Warren et al. (1998), and Casacchia et al. (2002); snow density values were defined following West et al. (1996), van den Broeke et al. (1999), and Albert et al. (2000); and snow grain-size values were defined following Gay et al. (2002). For elevations between 150 and 1500 m, parameter values were interpolated between the coastal and interior values. Blue-ice property values were defined to be independent of elevation, and followed those used by Liston et al. (1999b) for Jutulgryta. These parameter values are summarized in Table 1.

Meteorological station datasets provided the atmospheric forcing fields for the model simulations. We obtained Global Summary of the Day (GSOD) station data for the 10-yr period 1 July 1990–30 June 2000. The station distribution of these data is shown in Fig. 2. These points represent any station that contributed to the data archive and were used in the model simulations (e.g., year-round stations, summer-only stations, and stations that existed for intermittent time periods).

GSOD station observations of screen-height air temperature, relative humidity, and wind speed were inter-

TABLE 1. Snow and ice property data used in the model simulations. For the case of snow existing at elevations between 150 and 1500 m, the parameter values were linearly interpolated between the 150- and 1500-m values.

	Blue ice	Snow at elevations less than or equal to 150 m	Snow at elevations between 150 and 1500 m	Snow at elevations greater than or equal to 1500 m
Spectrally integrated albedo	0.65	0.80	Interpolated	0.90
Grain radius (mm)	5.00	0.35	Interpolated	0.15
Density (kg m^{-3})	800	550	Interpolated	300

polated to a grid covering Antarctica using MicroMet, a meteorological distribution model (Liston and Elder 2004, manuscript submitted to *J. Hydrometeor.*), MicroMet was also used to calculate the incoming solar and longwave radiation distributions. MicroMet interpolates irregularly distributed station observations to a regularly spaced grid using the Barnes objective analysis scheme (Barnes 1964, 1973; Koch et al. 1983). The Barnes scheme applies a Gaussian distance-dependent weighting function, where the weight that a station contributes to the overall value of the grid point decreases with increasing distance from the point. The interpolation weights are objectively determined as a function of the data spacing and distribution. In addition to the Barnes station interpolations, MicroMet employs corrections based on known temperature–elevation, wind–topography, and solar radiation–topography relationships (e.g., Dodson and Marks 1997). The resulting procedures produce much improved temperature, humidity, wind, and solar radiation distributions when the spatial scale of topographic variability is smaller than the distance between stations (Liston and Elder 2004, manuscript submitted to *J. Hydrometeor.*), which is the case for our Antarctic domain and GSOD station distribution. Incoming solar radiation fields were calculated assuming a cloud-cover fraction equal to that used in Liston et al. (1999b). GTOPO30, a global digital elevation model (DEM) with a horizontal grid spacing of 30 arc seconds (Gesch et al. 1999), was regridded to a 1.01-km increment and used for the MicroMet topographic corrections. The combination of the GSOD station data and the MicroMet distribution model produced the daily, spatially distributed atmospheric forcing data used to drive the energy-balance snow- and ice-melt model.

To define the Antarctic blue-ice and snow distributions, we used the maps provided by Winther et al. (2001). They mapped blue-ice areas using a NOAA/AVHRR Antarctic image mosaic established by the U.S. Geological Survey (Merson 1989; Ferrigno et al. 1996). The mosaic consists of 38 scenes acquired from 1980 to 1994. Winther et al. (2001) used AVHRR bands 1 (580–680 nm) and 2 (725–1100 nm) to create three blue-ice categories over Antarctica: melt-induced, wind-induced, and potential blue ice. Collectively these categories cover 239 902 km², or approximately 1.7% of Antarctica. Snow covers the remaining area (except for a small fraction of snow and ice free areas). This blue-ice and snow classification is available on a 1.01-km grid covering the Antarctic continent and ice shelves. For the model simulations presented herein, we assumed blue ice included all three blue-ice categories identified by Winther et al. (2001).

c. Model simulations

Simulating the surface and subsurface snow and ice melt over Antarctica required merging the meteorological forcing data, the snow/blue-ice distributions, and

the energy-balance melt/freeze model into a unified modeling system. Two independent model simulations were performed: one over the blue-ice areas and one over the snow areas. Both simulations span the 10-yr GSOD data record. Because of computational constraints, we were unable to run the modeling system over the 1.01-km blue-ice data grid. Instead, the MicroMet meteorological forcings were generated for all blue-ice areas using a 5-km grid and for all snow areas using a 10-km grid. We reasoned that it was acceptable to run the model over a coarser snow area grid than blue ice because the topography is generally less variable over Antarctic snow areas than blue-ice areas. In addition, because there is much greater snow area than blue ice, the snow simulations required a coarser grid to stay within available computational resources. Snow-area model integrations were also constrained to areas below 2500 m; we assumed areas higher than this never experience melting conditions, an assumption supported by our model simulations.

Using the blue-ice simulation as an example, we configured the energy-balance model with blue-ice parameter values (Table 1) and ran it over each 5-km MicroMet grid cell that coincided with one or more of the 1.01-km blue-ice cells. We then distributed the resulting model outputs over the 1.01-km blue-ice grid under the assumption that the 5-km meteorological forcings were valid over any blue-ice cells found within a 5-km cell. We repeated this procedure for the 10-km atmospheric forcing data and the 1.01-km snow-distribution data. Ultimately, this produced 1.01-km surface and subsurface melt distributions over the blue-ice and snow areas, in response to the 5- and 10-km gridded atmospheric forcings.

3. Results and discussion

a. Figures

The 10-yr averaged total annual surface and subsurface meltwater production for snow and blue-ice areas are shown in Fig. 4. Throughout the Antarctic coastal areas, some surface and subsurface melt was simulated. The annual total subsurface melt thickness in blue ice was on the order of 0.5 m. In contrast, the surface melt thickness for blue ice, and both the surface and subsurface melt thickness for snow, was on the order of 1 cm. The black-shaded parts of Figs. 4a and 4b correspond to blue-ice areas that had no simulated surface or subsurface melt. These areas are typically found in areas like the transantarctic mountain range and other high-elevation blue-ice areas like the upper Lambert Glacier. In addition, these roughly correspond to the wind-induced blue-ice areas identified by Winther et al. (2001). Seventy-nine percent of the blue-ice area produced simulated subsurface melt, while 42% of the blue-ice area produced simulated surface melt (Table 2). Table 2 presents the total amount of area that experienced simulated surface and subsurface melt in

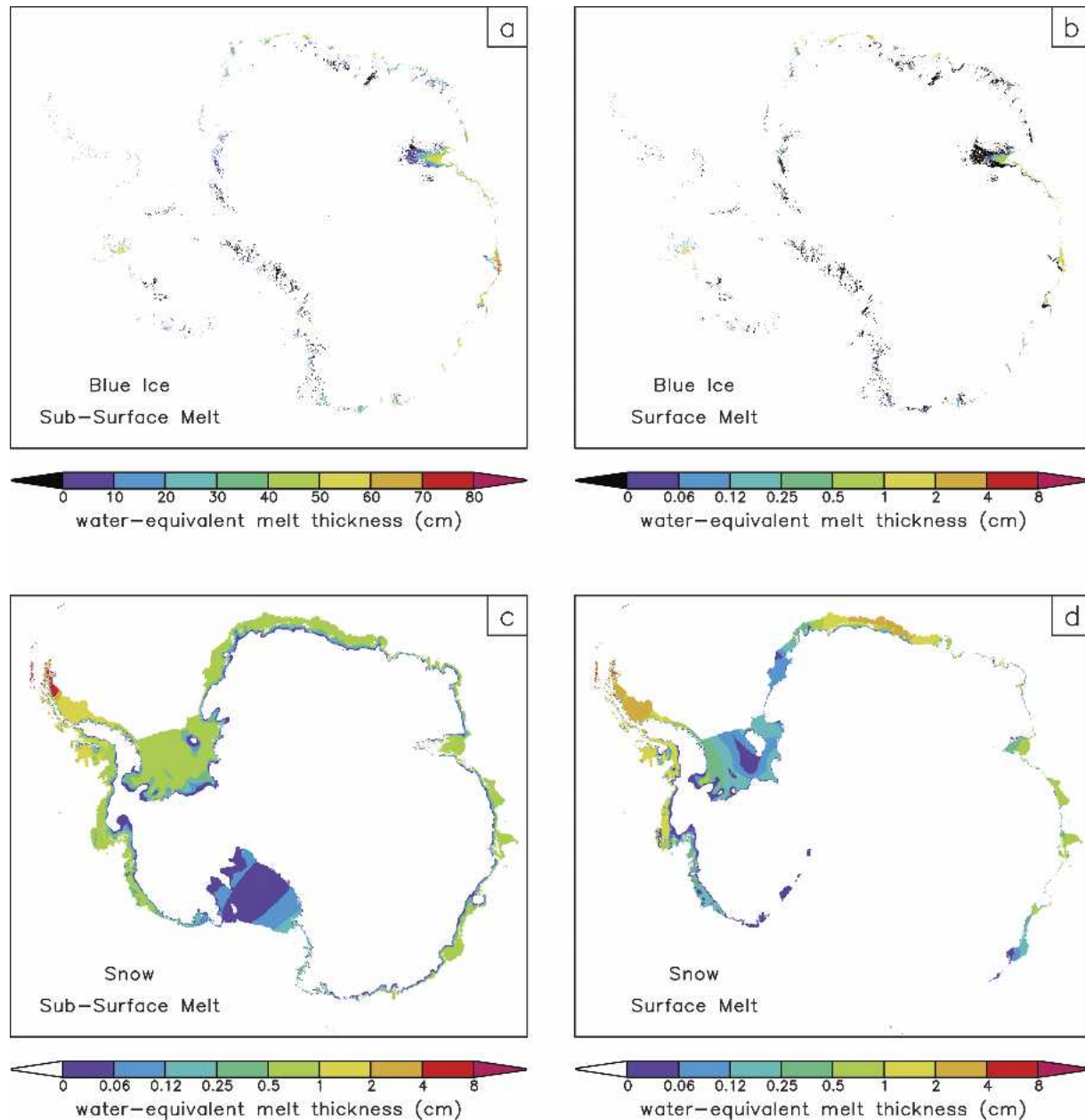


FIG. 4. The 10-yr averaged, annual Antarctic meltwater production for (a) blue-ice subsurface melt, (b) blue-ice surface melt, (c) snow subsurface melt, and (d) snow surface melt. (a), (b) The black-shaded regions are blue-ice areas with no simulated subsurface nor surface melt, respectively. Note that the data range for (a) is approximately 10 times greater than (b)–(d), and the (b)–(d) range is not linear in order to highlight variability in the lower values.

snow and blue-ice areas, and calculations of the Antarctic fraction represented by those areas. Blue-ice melt covered 1.4% of Antarctica, and snow-area melt covered 20.2% of Antarctica (the model simulations show that areas with surface melt also have subsurface melt).

Figures 4a and 4b illustrate that subsurface melt intensities in blue-ice areas were on the order of 10 times greater than blue-ice surface melt intensities. Further, the Lambert Glacier region constitutes a significant

proportion of the total Antarctic blue-ice melt fluxes. About one-third of the Antarctic blue-ice areas are found around the lower parts of the Lambert Glacier and in the vicinity of the Amery Ice Shelf (Winther et al. 2001). Figures 4c,d demonstrate that snow-covered areas affected by melt were much larger than those for blue ice. Note that snow-covered areas include snow located in transition zones between blue ice and dry (no melt features) snow. Thus, a large proportion of these

TABLE 2. Antarctic area experiencing melt, and the associated blue-ice area fraction and total Antarctic area fraction (based on a blue-ice area of 239 902 km² and an Antarctic area of 13 746 463 km²). Also shown is the 10-yr-averaged annual meltwater production.

	Area (10 ⁶ km ²)	Blue-ice fraction (%)	Antarctic fraction (%)	Meltwater production (km ³ yr ⁻¹)
Blue ice				
Surface melt	0.10	42.4	0.7	2.0
Subsurface melt	0.19	79.1	1.4	57.4
Snow				
Surface melt	1.53	—	11.1	46.0
Subsurface melt	2.77	—	20.2	316.5
Total				
Surface melt	1.63	—	11.8	48.0
Subsurface melt	2.96	—	21.6	373.9

snow areas may be composed of highly metamorphosed snow and firn and that any associated melt must play an important role in modifying snow characteristics like density and grain size. In an area like Jutulgryta, well-developed snow penitents with high density and low albedo can develop due to the strong incoming solar radiation and near-melting air temperatures. Figure 4a also shows that subsurface melt rates in blue ice were higher than surface and subsurface melt rates in snow (Figs. 4c,d).

In Figs. 4c and 4d, the Filchner–Ronne Ice Shelf (FRIS) exhibits both surface and subsurface melt while the Ross Ice Shelf (RIS) only exhibits subsurface melt. Below-surface ice layers on the RIS due to refreezing of meltwater have been detected on passive microwave satellite images (M. Fahnestock 2003, personal communication). The difference between the two ice shelves with respect to snow-surface melt is an indication that the FRIS is affected by melting episodes to a greater extent than the RIS area. This is not surprising in light of the recent regional warming and changes on the Antarctic Peninsula (De Angelis and Skvarca 2003). However, the simulated RIS subsurface melt under today's temperature conditions may indicate that this area could also experience surface melt under higher atmospheric temperatures. These and other simulated spatial melt variations on FRIS and RIS shown in Figs. 4c and 4d are the result of available meteorological station data and surface elevation variations: the modeling system contains no additional physics to create these patterns. Due to the lack of meteorological data on FRIS, the resulting melt distributions are primarily the result of the model-imposed temperature-related elevation variations. In contrast, the RIS melt patterns result from meteorological input variations.

The total daily, Antarctic meltwater production over the 10-yr simulation period is shown in Fig. 5. The subsurface meltwater production in blue-ice areas was relatively stable from year to year, and summer melt rates peaked at about 1.2 km³ day⁻¹. Blue-ice subsurface

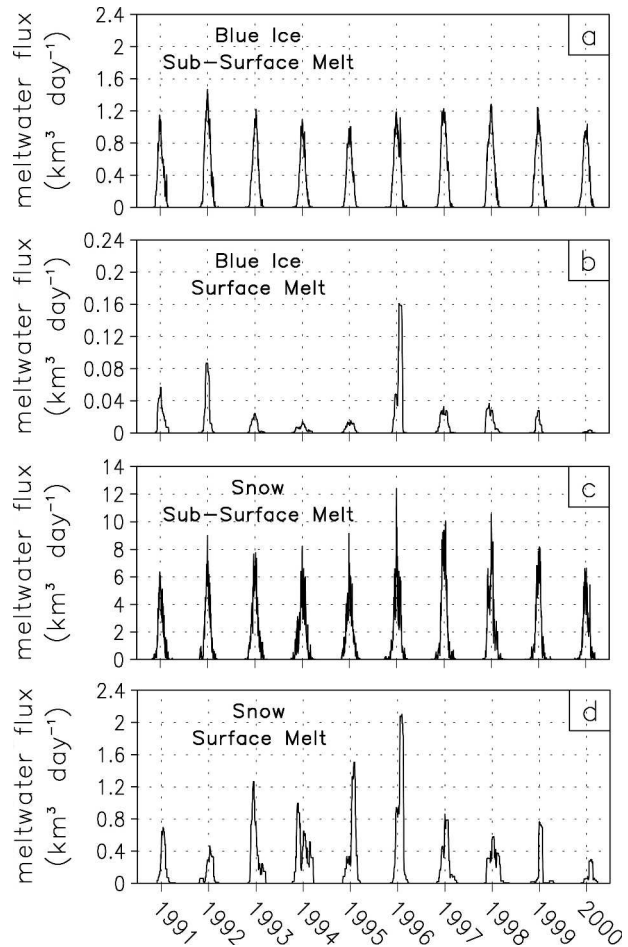


FIG. 5. Daily Antarctic meltwater production (in units of water volume) for (a) blue-ice subsurface melt, (b) blue-ice surface melt, (c) snow subsurface melt, and (d) snow surface melt. A 30-day line smoother was applied to the surface-melt curves to damp out the episodic nature of the surface melt and to make the surface melt fluxes readily comparable with the subsurface fluxes.

melt (Fig. 5a) was less variable and melt rates were typically 10–50 times greater than for blue-ice surface meltwater production. On average, meltwater production from snow surfaces was about 10 times greater than those from blue ice surfaces. In spite of the fact that the subsurface blue-ice meltwater flux is generally much greater than the subsurface snow meltwater flux (in areas experiencing similar atmospheric forcing), the snow areas cover a much greater spatial extent and consequently produce more total meltwater (Figs. 5c,d).

The greatest interannual variability in simulated melt fluxes occurs for the cases of snow and blue-ice surface melting (Fig. 5). Because conductive processes significantly govern the subsurface melt, shorter time-scale variations in surface atmospheric forcing (e.g., air temperature) are damped out, producing relatively smooth signals compared to that of surface melt. The simula-

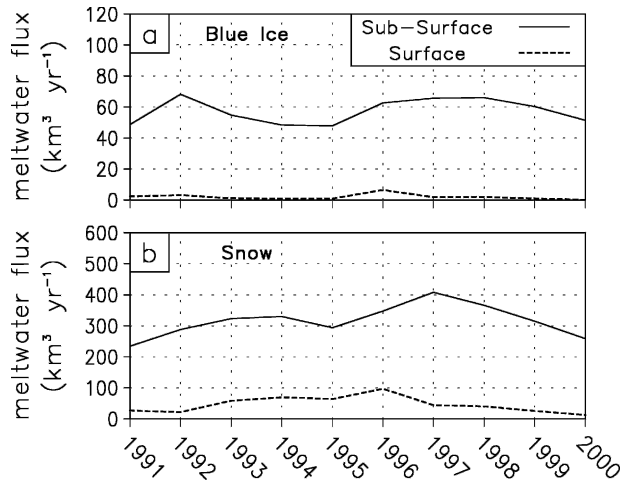


FIG. 6. Total annual subsurface and surface meltwater production (in units of water volume) within Antarctic (a) blue-ice and (b) snow areas.

tions calculated particularly high surface melt rates in 1996 (Figs. 5b,d), but the blue-ice subsurface melt production was not notably enhanced during that year (Fig. 5a). One explanation for this is that solar radiation is the dominant driving force for subsurface melting while sensible and latent heat fluxes significantly affect the surface melt. This reasoning suggests that surface melt production would be a better indicator of increasing atmospheric temperature trends than subsurface melt production.

Figure 6 shows the total annual subsurface and surface meltwater production within Antarctic blue-ice and snow areas (obtained by integrating the daily values for each year in Fig. 5). Values averaged over the 10-yr simulation period are given in Table 2. Average annual subsurface blue-ice melt production was $57 \text{ km}^3 \text{ yr}^{-1}$. For subsurface melt in snow areas this number was approximately 6 times higher, at $317 \text{ km}^3 \text{ yr}^{-1}$. The surface melt in snow-covered areas was comparable to the subsurface blue-ice melt, with an annual average of $46 \text{ km}^3 \text{ yr}^{-1}$. The greater interannual surface-melt variability seen in Fig. 5 is masked in Fig. 6 because the surface fluxes are much smaller than the subsurface fluxes. While the melt-production rates (at any given location) are substantially less in the snow areas than in the blue-ice areas (Fig. 4), the total Antarctic melt volume in the snow areas is much greater than in the blue-ice areas because the contributing snow area is much greater (approximately 15 times greater, under the assumption that the surface melt areas are a subset of the subsurface melt areas) than the contributing blue-ice area (Table 2).

The total meltwater production in both blue-ice and snow areas was $422 \text{ km}^3 \text{ yr}^{-1}$ (Table 2). This amount of meltwater is comparable to 1000 icebergs with dimensions $1 \text{ km} \times 1 \text{ km}$ with an ice thickness of about 500 m. If the simulated meltwater had produced runoff reach-

ing the ocean, this would be a significant Antarctic mass-balance budget term. However, we believe it is appropriate to assume most of the produced meltwater refreezes close to where it was produced (as assumed in the model). Therefore, the subsurface and surface melt processes primarily impact the Antarctic surface energy budget through the addition of the melt term (e.g., Liston 2004). Another way to illustrate the significance of this $422 \text{ km}^3 \text{ yr}^{-1}$ meltwater production is to uniformly distribute this quantity over all of Antarctica ($13\,746\,463 \text{ km}^2$; Table 2), yielding an area-mean melt rate of 31 mm yr^{-1} .

Figure 7 shows the 10-yr averaged, total number of days in a year exhibiting subsurface and surface melt for blue-ice and snow-covered areas. Subsurface melt in both snow and blue-ice occurs more than 45 days per year over much of the Antarctic coast. This is due to the simulated solid-state greenhouse effect presented by Brandt and Warren (1993) and how it varies with snow and ice grain size, density, and albedo characteristics (Table 1). In contrast, surface melt in both snow and blue-ice typically occurs only a few days, or less. This is because Antarctic near-surface air temperatures are generally below freezing. Interestingly, the period with subsurface snowmelt on the FRIS lies between 15 and 60 days, while it is between 0 and 15 days on the RIS. Also, on the FRIS there is a tendency toward longer periods of melt on the western part of the ice shelf. In contrast, we do not find any spatial variability on the RIS.

Zwally and Fiegles (1994) used passive-microwave data to calculate an "annual Antarctic melt index," defined to be the product of the area experiencing melt and the melt duration. They found a 9-yr (1978–87) average of $24 \times 10^6 \text{ day km}^2$. Torinesi et al. (2003) repeated these calculations for a 20-yr period (1980–99) and calculated an average of $27 \times 10^6 \text{ day km}^2$. For comparison, we followed this approach and calculated indices for surface and subsurface melting using our model outputs (Fig. 8). Our 10-yr average was $5 \times 10^6 \text{ day km}^2$ for surface melting and $101 \times 10^6 \text{ day km}^2$ for subsurface melting. Our methods to arrive at index values are very different from those of Zwally and Fiegles (1994) and Torinesi et al. (2003). In their studies, melting is assumed to occur if the microwave brightness temperature increases by a fixed threshold above the time series average brightness temperature for a given location. In addition, Zwally and Fiegles (1994) calculated values using a 30-km grid increment (25 km for Torinesi et al. 2003), while we used a 1.01-km grid. While Zwally and Fiegles (1994) and Torinesi et al. (2003) refer to their melt as "surface melting," the passive-microwave signal is responding to both surface and near-surface (or subsurface) moisture and snow/ice conditions. Since our calculated surface melt areas are generally coincident with subsurface melt areas, we conclude that the Zwally and Fiegles (1994) and Torinesi et al. (2003) values can be most directly compared

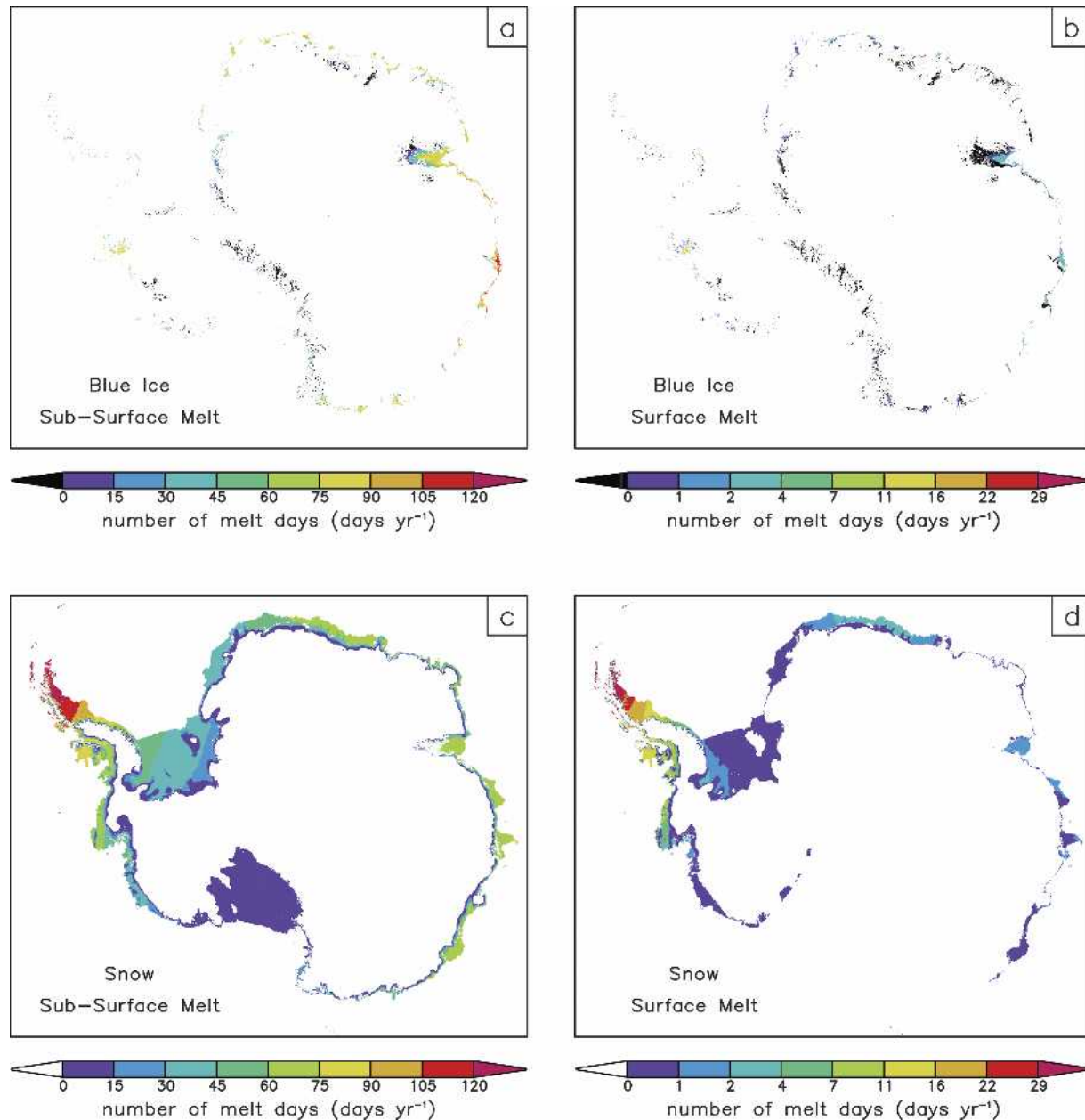


FIG. 7. The 10-yr averaged, total number of days in a year that had (a) blue-ice subsurface melt, (b) blue-ice surface melt, (c) snow subsurface melt, and (d) snow surface melt. (a), (b) The black-shaded regions are blue-ice areas with no simulated subsurface nor surface melt, respectively. Note that the data range for (a), (c) is approximately 4 times greater than (b), (d), and the (b)–(d) range is not linear in order to highlight variability in the lower values.

with our subsurface melt values. Thus, our average melt index is 4.2 and 3.7 times greater than those of Zwally and Fiegles (1994) and Torinesi et al. (2003), respectively.

b. Model limitations

In spite of our general satisfaction with these model results, it is important to be clear about the assumptions

and potential deficiencies of this modeling study. These simulations have assumed that there are only two kinds of frozen water located in the top 15 m of Antarctica's glaciers, ice shelves, and ice sheets: snow and blue ice. We have assumed that these two cover types have temporally constant and elevation-dependent properties of density, grain size, and albedo (Table 1). In reality, variables such as slope, aspect, distance from the coast and mountains, accumulation rate, and wind regime can all

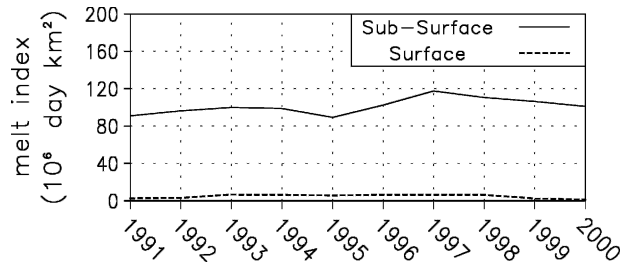


FIG. 8. Annual Antarctic melt index, defined to be the product of the area experiencing melting and the duration of that melting (Zwally and Fiegles 1994; Torinesi et al. 2003). Indices are shown for subsurface and surface melting, where each of these is for the combined blue-ice and snow areas.

influence these parameters to varying degrees. In addition, we have assumed that the Antarctic cloud-cover fraction is spatially and temporally constant. In the natural system, there are possibly important seasonal and spatial variations in all of these snow, ice, and atmospheric properties. Unfortunately, adequate observations and/or models to define these variations do not exist.

The atmospheric forcings over snow and blue-ice were defined on a 10- and 5-km grid, respectively. We used this to drive the melt models over the AVHRR 1.01-km gridded snow and blue-ice distribution dataset, thus accounting for the snow and blue-ice distributions that were subgrid to the atmospheric forcings. While it would have been most desirable to supply the atmospheric forcing on the 1.01-km snow and blue-ice grid, both computer memory, storage, and processor constraints did not allow this. We also recognize that the use of daily-averaged atmospheric forcing variables, instead of, say, hourly values, will produce a smoothing of the natural system. While hourly data are available for some Antarctic stations, for this spatially distributed study we have elected to use daily data in order to achieve the greatest possible spatial detail and coverage.

During the model simulations, we assumed it was appropriate to let all three of the blue-ice categories (melt induced, wind induced, and potential) mapped by Winther et al. (2001) define where blue-ice existed. While it was clearly appropriate to define blue-ice to include the melt-induced and wind-induced blue ice, the decision to include potential blue ice was more ambiguous. Winther et al. (2001) noted that this potential blue ice comprises probably less than 50% blue ice. Thus, blue-ice meltwater production in Figs. 5 and 6, and Table 2, could be reduced by approximately one-third in order to account for possible snow within potential blue-ice areas.

4. Conclusions

Since the energy balance model was developed and tested using an extensive in situ dataset (Liston et al.

1999b), we have confidence that the model does a reasonable job of reproducing melt fluxes. At first, we were surprised by the extent and magnitude of subsurface melt, but conclude now that its significance has previously not been sufficiently recognized due to the hidden nature of this process. According to model simulations, 20.2% and 1.4% of Antarctica exhibited subsurface melt in snow-covered and blue-ice areas, respectively. The corresponding Antarctic fractions for surface melt were 11.1% and 0.7%, respectively.

Because of their large spatial extent, total meltwater production in snow-covered areas was much higher than blue-ice areas (i.e., 362.5 cf. 59.4 km³ yr⁻¹). This occurred in spite of the fact that, at any given location, meltwater production and the thickness of the subsurface melt layer were higher in blue-ice areas. In blue-ice areas, almost 30 times more meltwater was produced subsurface than at the surface. For snow-covered areas, about 7 times more meltwater was produced subsurface compared to the surface. This suggests that both subsurface and surface melt must be accounted for when studying so-called surface melt in Antarctica.

Another interesting feature of our model simulations are the interannual surface melt flux variations. The year 1996 stands out as one with the greatest surface meltwater production. Subsurface melt fluxes do not vary much from year to year because they are strongly controlled by conductive processes. Thus, short-term temperature variations have less impact on subsurface than surface melt. Following this rationale, we think a change in surface melt fluxes is a better indicator of climate fluctuations than changes in subsurface melt fluxes.

The “annual Antarctic melt index,” defined as the product of the area experiencing melt and the melt duration, can be used to quantify the degree of Antarctic surface melt. Our 10-yr average data indicated a melt index of 5×10^6 day km² for surface melt and 101×10^6 day km² for subsurface melt. The simulations showed regional variations in the melt duration; for example, annual average melt periods are between 15 and 60 days on the FRIS and between 0 and 15 days on the RIS. By monitoring such variations it should be possible to detect and track regional and continental signatures of Antarctic climate change.

Finally, we report surface and subsurface meltwater production values that equate to 31 mm yr⁻¹ if distributed evenly over the whole of Antarctica. If this meltwater had produced runoff to the ocean it would have represented a significant component of the Antarctic mass balance. However, most of this meltwater re-freezes close to where it was formed. Thus, this study is primarily a contribution to improving our understanding of the Antarctic surface energy balance and the evolution of surface and near-surface snow characteristics.

Acknowledgments. The authors thank Martin Nørman Jespersen for providing the blue-ice distribution data; this work could not have been completed without his assistance. We also thank Michiel R. van den Broeke, Mark A. Fahnestock, and Andrew G. Fountain for their insightful reviews of this paper. Financial support was provided by the Norwegian Research Council and the Norwegian Polar Institute.

REFERENCES

- Albert, M. R., E. F. Shultz, and F. E. Perron, 2000: Snow and firm permeability at Siple Dome, Antarctica. *Ann. Glaciol.*, **31**, 353–356.
- Barnes, S. L., 1964: A technique for maximizing details in numerical weather map analysis. *J. Appl. Meteor.*, **3**, 396–409.
- , 1973: Mesoscale objective map analysis using weighted time-series observations. NOAA Tech. Memo. ERL NSSL-69, National Severe Storms Laboratory, Norman, OK, 60 pp.
- Bingham, A. W., and M. R. Drinkwater, 2000: Recent changes in the microwave scattering properties of the Antarctic ice sheet. *IEEE Trans. Geosci. Remote Sens.*, **38**, 1810–1820.
- Bintanja, R., 1999: On the glaciological, meteorological and climatological significance of Antarctic blue-ice areas. *Rev. Geophys.*, **37**, 337–359.
- Birnie, R. V., and J. E. Gordon, 1980: Drainage systems associated with snow melt, South Shetland Islands, Antarctica. *Geogr. Ann.*, **62A** (1-2), 57–62.
- Bøggild, C. E., J.-G. Winther, K. Sand, and H. Elvehøy, 1995: Sub-surface melting in blue-ice fields in Dronning Maud Land, Antarctica: Observations and modeling. *Ann. Glaciol.*, **21**, 162–168.
- Brandt, R. E., and S. G. Warren, 1993: Solar-heating rates and temperature profiles in Antarctic snow and ice. *J. Glaciol.*, **39** (131), 99–110.
- Brun, E., E. Martin, V. Simon, C. Gendre, and C. Coleou, 1989: An energy and mass model of snow cover suitable for operational avalanche forecasting. *J. Glaciol.*, **35** (121), 333–342.
- Casacchia, R., R. Salvatori, A. Cagnati, M. Valt, and S. Ghergo, 2002: Field reflectance of snow/ice covers at Terra Nova Bay, Antarctica. *Int. J. Remote Sens.*, **23**, 4653–4667.
- Chinn, T. J., 1993: Physical hydrology of the Dry Valley lakes. *Physical and Biogeochemical Processes in Antarctic Lakes*, W. J. Green and E. I. Friedmann, Eds., Antarctic Research Series, Vol. 59, Amer. Geophys. Union, 1–51.
- Colbeck, S. C., 1989: Snow-crystal growth with varying surface temperatures and radiation penetration. *J. Glaciol.*, **35** (119), 23–29.
- Dana, G. L., R. E. Davis, A. G. Fountain, and R. A. Wharton, 2002: Satellite-derived indices of stream discharge in Taylor Valley, Antarctica. *Hydrol. Processes*, **16**, 1603–1616.
- De Angelis, H., and P. Skvarca, 2003: Glacier surge after ice shelf collapse. *Science*, **299**, 1560–1562.
- Dodson, R., and D. Marks, 1997: Daily air temperature interpolated at high spatial resolution over a large mountainous region. *Climate Res.*, **8**, 1–20.
- Fahnestock, M. A., W. Abdalati, and C. A. Shuman, 2002: Long melt seasons on ice shelves of the Antarctic Peninsula: An analysis using satellite-based microwave emission measurements. *Ann. Glaciol.*, **34**, 127–133.
- Ferrigno, J. G., J. L. Mullins, J. Stapleton, P. S. Chavez Jr., M. G. Velasco, R. S. Williams Jr., G. F. Delinski Jr., and D. Lear, 1996: Satellite image map of Antarctica. USGS Miscellaneous Field Investigations Map I-2560, U.S. Geological Survey, Washington, DC, 1 p.
- Fountain, A. G., G. Dana, K. J. Lewis, B. H. Vaughn, and D. McKnight, 1998: Glaciers of the McMurdo Dry Valleys, Southern Victoria Land, Antarctica. *Ecosystem Processes in a Polar Desert: The McMurdo Dry Valleys, Antarctica*, J. Prisco, Ed., Antarctic Research Series, Vol. 2, Amer. Geophys. Union, 65–75.
- Gay, M., M. Fily, C. Genthon, M. Frezzotti, H. Oerter, and J.-G. Winther, 2002: Snow grain-size measurements in Antarctica. *J. Glaciol.*, **48** (163), 527–535.
- Gesch, D. B., K. L. Verdin, and S. K. Greenlee, 1999: New land surface digital elevation model covers the Earth. *Eos, Trans. Amer. Geophys. Union*, **80**, 69–70.
- Grenfell, T. C., S. G. Warren, and P. C. Mullen, 1994: Reflection of solar-radiation by the Antarctic snow surface at ultraviolet, visible, and near-infrared wavelengths. *J. Geophys. Res.*, **99** (D9), 18 669–18 684.
- Hardy, D., M. W. Williams, and C. Escobar, 2001: Near-surface faceted crystals, avalanches and climate in high-elevation, tropical mountains of Bolivia. *Cold Reg. Sci. Technol.*, **33** (2–3), 291–302.
- Jezek, K. C., 1999: Glaciological properties of the Antarctic ice sheet from RADARSAT-1 synthetic aperture radar imagery. *Ann. Glaciol.*, **29**, 286–290.
- Koch, S. E., M. desJardins, and P. J. Kocin, 1983: An interactive Barnes objective map analysis scheme for use with satellite and conventional data. *J. Climate Appl. Meteor.*, **22**, 1487–1503.
- Koh, G., and R. Jordan, 1995: Sub-surface melting in a seasonal snow cover. *J. Glaciol.*, **41** (139), 474–482.
- Lewis, K. J., A. G. Fountain, and G. L. Dana, 1998: Surface energy balance and meltwater production for a dry valley glacier, Taylor Valley, Antarctica. *Ann. Glaciol.*, **27**, 603–609.
- Liston, G. E., 2004: Representing subgrid snow cover heterogeneities in regional and global models. *J. Climate*, **17**, 1381–1397.
- , O. Bruland, J.-G. Winther, H. Elvehøy, and K. Sand, 1999a: Meltwater production in Antarctic blue-ice areas: Sensitivity to changes in atmospheric forcing. *Polar Res.*, **18** (2), 283–290.
- , J.-G. Winther, O. Bruland, H. Elvehøy, and K. Sand, 1999b: Below-surface ice melt on the coastal Antarctic ice sheet. *J. Glaciol.*, **45** (150), 273–285.
- , —, —, —, —, and L. Karlöf, 2000: Snow and blue-ice distribution patterns on the coastal Antarctic Ice Sheet. *Antarct. Sci.*, **12** (1), 69–79.
- Merson, R. H., 1989: An AVHRR mosaic image of Antarctica. *Int. J. Remote Sens.*, **10** (4–5), 669–674.
- Orheim, O., and B. K. Lucchitta, 1990: Investigating climate change by digital analysis of blue ice extent on satellite images of Antarctica. *Ann. Glaciol.*, **14**, 211–215.
- Paige, R. A., 1968: Sub-surface melt pools in the McMurdo Ice Shelf, Antarctica. *J. Glaciol.*, **7** (51), 511–516.
- Phillips, H. A., 1998: Surface meltstreams on the Amery Ice Shelf, East Antarctica. *Ann. Glaciol.*, **27**, 177–181.
- Rau, F., and M. Braun, 2002: The regional distribution of the dry-snow zone on the Antarctic Peninsula north of 70 degrees S. *Ann. Glaciol.*, **34**, 95–100.
- Ridley, J., 1993: Surface melting on Antarctic Peninsula ice shelves detected by passive microwave sensors. *Geophys. Res. Lett.*, **20**, 2639–2642.
- Scambos, T. A., C. Hulbe, M. Fahnestock, and J. Bohlander, 2000: The link between climate warming and break-up of ice shelves in the Antarctic Peninsula. *J. Glaciol.*, **46** (154), 516–530.
- Schlatter, T. W., 1972: The local surface energy balance and sub-surface temperature regime in Antarctica. *J. Appl. Meteor.*, **11**, 1048–1062.
- Shepherd, A., D. Wingham, T. Payne, and P. Skvarca, 2003: Larsen ice shelf has progressively thinned. *Science*, **302** (5646), 856–859.
- Torinesi, O., M. Fily, and C. Genthon, 2003: Variability and trends of the summer melt period of Antarctic ice margins since 1980 from microwave sensors. *J. Climate*, **16**, 1047–1060.

- van den Broeke, M. R., J.-G. Winther, E. Isaksson, F. Pinglot, T. Eiken, and L. Karlof, 1999: Climate variables along a traverse line in Dronning Maud Land, East Antarctica. *J. Glaciol.*, **45** (150), 295–302.
- , C. H. Reijmer, and R. S. W. van de Wal, 2005: A study of the surface mass balance in Dronning Maud Land, Antarctica, using automatic weather stations. *J. Glaciol.*, in press.
- Warren, S. G., R. E. Brandt, and P. O. Hinton, 1998: Effect of surface roughness on bidirectional reflectance of Antarctic snow. *J. Geophys. Res.*, **103** (E11), 25 789–25 807.
- West, R. D., D. P. Winebrenner, L. Tsang, and H. Rott, 1996: Microwave emission from density-stratified Antarctic firn at 6 cm wavelength. *J. Glaciol.*, **42** (140), 63–76.
- Winther, J.-G., 1993: Studies of snow surface characteristics by Landsat TM in Dronning Maud Land, Antarctica. *Ann. Glaciol.*, **17**, 27–34.
- , 1994: Spectral bi-directional reflectance of snow and glacier ice measured in Dronning Maud Land, Antarctica. *Ann. Glaciol.*, **20**, 1–5.
- , H. Elvehøy, C. E. Bøggild, K. Sand, and G. E. Liston, 1996: Melting, runoff and the formation of frozen lakes in a mixed snow and blue-ice field in Dronning Maud Land, Antarctica. *J. Glaciol.*, **42** (141), 271–278.
- , M. N. Jespersen, and G. E. Liston, 2001: Blue-ice areas in Antarctica derived from NOAA AVHRR satellite data. *J. Glaciol.*, **47**, 325–334.
- Zwally, H. J., and S. Fiegles, 1994: Extent and duration of Antarctic surface melting. *J. Glaciol.*, **40**, 463–476.